

See discussions, stats, and author profiles for this publication at: <https://www.researchgate.net/publication/231652914>

# Long-Range Interfacial Electrochemical Electron Transfer of *Pseudomonas aeruginosa* Azurin–Gold Nanoparticle Hybrid Systems

ARTICLE in THE JOURNAL OF PHYSICAL CHEMISTRY C · JULY 2009

Impact Factor: 4.77 · DOI: 10.1021/jp902611x

---

CITATIONS

24

READS

49

## 4 AUTHORS, INCLUDING:



[Qijin Chi](#)

Technical University of Denmark

98 PUBLICATIONS 2,299 CITATIONS

[SEE PROFILE](#)



[Jingdong Zhang](#)

Technical University of Denmark

100 PUBLICATIONS 2,297 CITATIONS

[SEE PROFILE](#)

# Long-Range Interfacial Electrochemical Electron Transfer of *Pseudomonas aeruginosa* Azurin–Gold Nanoparticle Hybrid Systems

Palle S. Jensen, Qijin Chi, Jingdong Zhang, and Jens Ulstrup\*

Department of Chemistry and Nano•DTU, Building 207, Technical University of Denmark, DK-2800 Lyngby, Denmark

Received: March 23, 2009; Revised Manuscript Received: May 26, 2009

We have prepared a “hybrid” of the blue copper protein azurin (*Pseudomonas aeruginosa*) and a 3 nm gold nanoparticle (AuNP). The AuNP/azurin hybrid was assembled on a Au(111)-electrode surface in a two-step process. The AuNP was first attached to the Au(111) electrode via Au–S chemisorption of a 4,4'-biphenyldithiol (4,4'-BPDT) monolayer. This was followed by 1-decanethiol modification of the bound AuNP and hydrophobic binding of azurin to the AuNP. The Au(111)/AuNP/azurin system was characterized by atomic force microscopy (AFM), cyclic voltammetry (CV), and *in situ* electrochemical scanning tunneling microscopy (*in situ* STM). AFM and STM point to the feasibility of preparing both dense and sparsely populated AuNP monolayers. CV shows two pairs of voltammetric peaks at high scan rates, both around the azurin equilibrium potential. One pair of redox peaks follows closely that of azurin hydrophobically immobilized directly on a Au(111)/1-tetradecanethiol reference surface. The other pair, tentatively assigned to the AuNP/azurin hybrid, shows a 20-fold electron transfer rate enhancement over the reference system. This dual pattern is supported by *in situ* STM which shows two distinct contrasts. A strong contrast most likely arises either from azurin-free AuNPs or from AuNP-free azurin displaced onto the Au(111)/4,4'-BPDT surface. The other contrast, assigned to the AuNP/azurin hybrid, is weaker and fluctuates in time. Mechanisms of electronic conductivity of the AuNP/azurin system are discussed.

## 1. Introduction

Metallic and semiconductor nanoparticles (NPs) in narrow size distributions from 1 to 100 nm are broadly important in the fields of catalysis and electrocatalysis, as chemical and biological markers, in electroanalysis, and in other areas.<sup>1–10</sup> Their variable size and electronic properties all the way from molecular to almost bulk size have prompted intense interest in metallic NPs as versatile building blocks in nanoscale electronics and other nanotechnology.<sup>11</sup>

NP synthesis and physical-chemical characterization is presently broadly developed. Particularly, the preparation of NPs coated with protecting molecular monolayers such as functionalized alkanethiols has offered a solid basis for a detailed understanding of optical and electronic properties of NPs and NP networks.<sup>2,3,6,12–14</sup> Molecular coating has also opened ways to NP immobilization including organization in two-dimensional patterns on metallic electrode surfaces which offer at the same time efficient electrochemical approaches to NP electronic function.<sup>15–18</sup>

Noble metal NPs and nanoscale surface structures are efficient heterogeneous catalysts and electrocatalysts for a variety of chemical and electrochemical processes including processes of technological importance.<sup>19</sup> In fundamental respects, noble metallic NPs, particularly 1.5–20 nm AuNPs, have emerged as electrocatalysts for both simple interfacial electron transfer (ET) processes<sup>8–10</sup> and composite bioelectrochemical processes. The latter involve both small redox metalloproteins (cytochrome *c*)<sup>18,20,21</sup> and AuNP-mediated electrocatalysis by larger redox enzymes. These are associated with more sophisticated catalytic

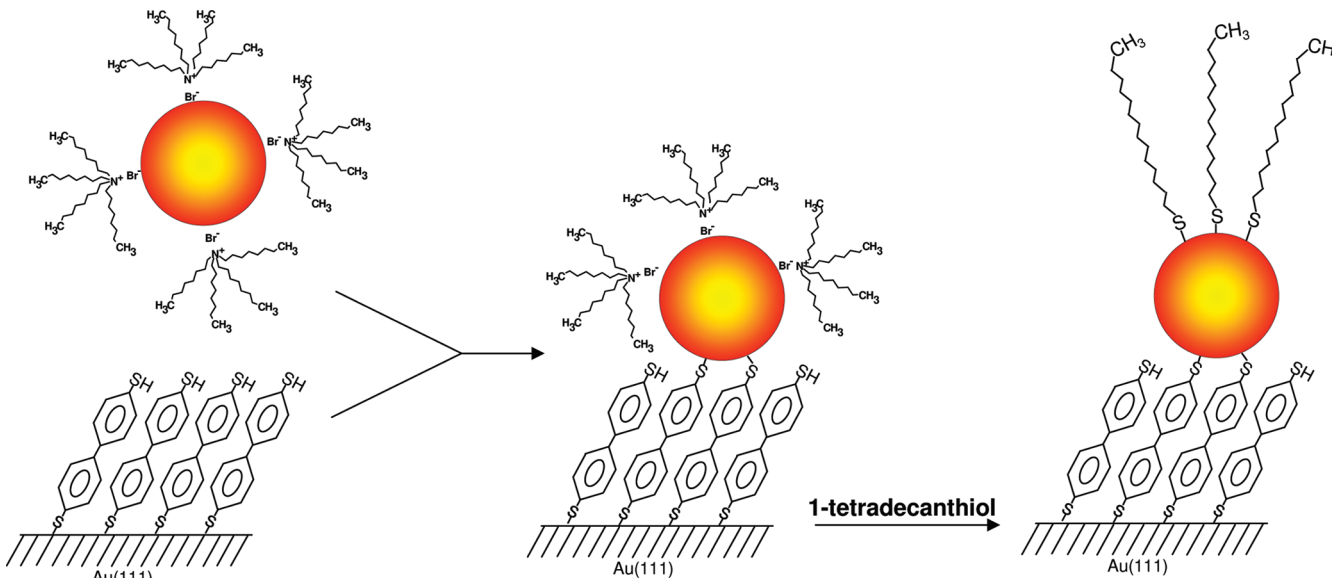
function but closely based on ET and electronic conductivity through the enzyme molecules.<sup>22,23</sup>

In most of these cases, the NP is integrated as a covalently or noncovalently bound structural unit of a molecular linker of variable length and chemical composition that attaches the protein or enzyme to the electrode surface. The notion of bioinorganic “hybrids” is sometimes used for the structures that integrate the inorganic NP and the biomolecule. The exact function of the NP is presently not clarified except that the NP significantly enhances the rate of interfacial electrochemical ET in spite of a strongly increased total distance between the redox center and the electrode surface. Highly efficient interfacial ET between the NP and either electrode or the (bio)molecules must be crucial, but the physical origin of this effect presently eludes precise identification. The effect is reminiscent both of the strong interfacial field enhancement of the surface plasmon delocalization that leads to surface-enhanced Raman scattering<sup>24,25</sup> and of coherent multi-ET as observed in single-molecule conductivity of redox molecules.<sup>26,27</sup>

In addition to NP-promoted biological long-range interfacial ET, stoichiometrically well-defined NP–biomolecular hybrids have been reported. Willner and associates reported the notion of an “electrical nanoplug” in which a 1.4 nm AuNP was integrated into a conductive film to yield a highly efficient electrical contact with the electrode support.<sup>22</sup> Abad and associates reported a strategy for immobilization of a genetically engineered horseradish peroxidase/ferredoxin/NADP<sup>+</sup> complex onto a 3 nm AuNP, creating a fully functional AuNP/linker/protein hybrid.<sup>28</sup> Aubin-Tam and Hamad-Schifferli described a “hybrid” between a variably coated 1.4 nm AuNP and yeast cyt *c* linked to the AuNP via the Cys102 residue close to the protein surface.<sup>29</sup> Circular dichroism spectroscopy showed that the protein structure was broadly retained but affected by the

\* To whom correspondence should be addressed. E-mail: ju@kemi.dtu.dk.

**SCHEME 1: Schematic Representation of Gold Nanoparticle Immobilization on Dithiol-Modified Au(111) Surfaces and Subsequent Modification of the Gold Nanoparticle Surface<sup>a</sup>**

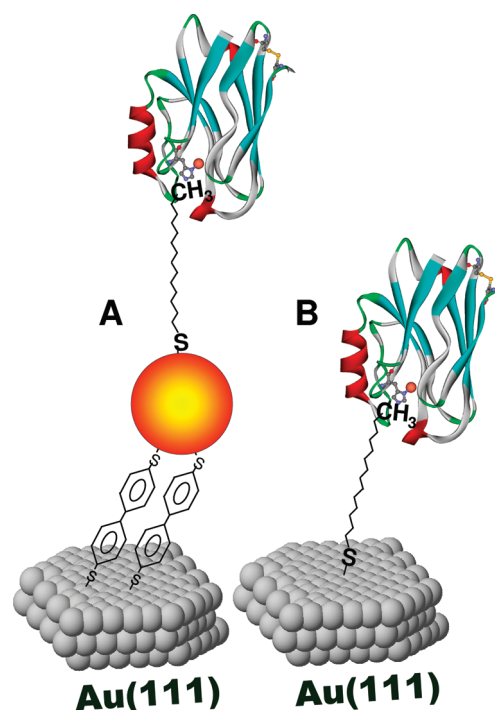


<sup>a</sup> Not drawn to scale.

molecular nature of the AuNP coating layer. A 1:1 stoichiometric complex between horse heart cyt *c* and a 3 nm 6,8-dithiocic acid (TA)-coated AuNP was finally described in our previous report.<sup>18</sup> The coated NP is strongly negatively charged at pH 7 due to deprotonation of the terminal carboxylic acid groups. Binding to strongly positively charged cyt *c* is electrostatic but strong enough to ensure robust 1:1 hybrid formation. Fast NP–protein electron exchange through the TA coating layer was further suggested by absorption spectral features of the hybrid entity.

In the present report, we address NP/protein hybrid formation and NP-enhanced redox protein interfacial ET in a different way. Three nm AuNPs stabilized by the phase transfer reagent, tetraoctylammonium bromide ((TOA)Br), were linked directly to a 4,4'-biphenyldithiol (BPDT) self-assembled monolayer on a Au(111)-electrode surface. The choice of this linker molecule was prompted by a recent comprehensive study<sup>30</sup> and chosen as a representative of a group of variable-length aromatic thiol-linked molecules with high single-molecule conductances (2.8 nS/molecule). (TOA)Br was then displaced by 1-tetradecanethiol (Scheme 1), leaving a strongly hydrophobic NP surface exposed to the aqueous solution. This was followed by linking the target redox metalloprotein, azurin, to the immobilized, hydrophobically coated AuNP. This linking mode ensures that the Cu center of azurin faces the NP surface (Scheme 2) and has been highly successful in hydrophobic linking of fully active azurin directly to variable-length alkanethiol-modified Au(111)-electrode surfaces.<sup>31,32</sup> As a Au–S/hydrophobic linker, 1-tetradecanethiol attaches azurin on the single-crystal Au(111)-electrode surface in configurations highly favorable for interfacial electrochemical ET through the linker molecules, and with both insignificant capacitive background currents and virtual absence of inhomogeneous broadening of the cyclic voltammograms otherwise nearly always observed in protein voltammetry.<sup>31,32</sup> At the same time, the length of this linker molecule is in the range where cyclic voltammetry of hydrophobically linked azurin shows clear kinetically (tunneling) controlled interfacial ET. The molecule is therefore well suited as a linker of choice for addressing AuNP catalytic enhancement of interfacial electrochemical ET of azurin. The AuNP array was characterized by atomic force

**SCHEME 2: Schematic Illustration of the Molecular Assembly of Azurin on Au(111) Surfaces: (A) Azurin–Nanoparticle Hybrid Structure on the Au(111) Surface; (B) Reference System without Gold Nanoparticles<sup>a</sup>**



<sup>a</sup> For simplicity, capping ligands on the AuNPs are mostly omitted.

microscopy (AFM) and *in situ* scanning tunneling microscopy (STM). The AuNP/azurin surfaces were first characterized by cyclic voltammetry that disclosed both significant interfacial ET enhancement compared to the azurin reference system without NPs and an intriguing dual voltammetric pattern. The AuNP/azurin hybrids on the Au(111)-electrode surface were, second, mapped by *in situ* STM to single-molecule resolution. Two distinct contrast features suggest that AuNP/azurin hybrids and

either azurin-free AuNPs or AuNP-free azurin molecules are both present on the Au(111)-electrode surface.

## 2. Experimental Section

**Materials and Chemicals.** The Au(111) electrodes used for electrochemical and STM measurements were homemade and pretreated before use as described.<sup>31–33</sup> Gold on glass samples were purchased from Arrandee, Germany.

The following chemicals were used as received: HAuCl<sub>4</sub>·3H<sub>2</sub>O (>99% Sigma-Aldrich), NaBH<sub>4</sub> (>99.9%, Sigma-Aldrich), chloroform (>99.8%, Sigma-Aldrich), tetra-octylammonium bromide ((TOA)Br) (>98%, Fluka), toluene (>99.9%, Sigma-Aldrich), tetrahydrofuran (THF) (>99.9%, Aldrich), H<sub>2</sub>SO<sub>4</sub> (Suprapur, Merck), ethanol (>99.9%, Merck), NaHCO<sub>3</sub> (>99.7%, Fluka), 1-tetradecanethiol (>98%, Fluka), 4,4'-biphenyldithiol (>98%, TCI Europe), and 4-mercaptopbenzoic acid (>95%, TCI Europe). *Pseudomonas aeruginosa* azurin (Az) from Sigma-Aldrich was purified by high performance liquid chromatography (HPLC) as reported.<sup>34</sup> The azurin concentration was determined by UV-vis spectroscopy (HP8453 Instrument) with a molar absorption coefficient of 5700 M<sup>-1</sup> cm<sup>-1</sup> at 628 nm. Buffered azurin solutions were stored at -20 °C. Distilled water purified through a Milli-Q system (18.2 MΩ cm, Millipore housing) was used throughout.

**Synthesis of Gold Nanoparticles.** AuNPs were synthesized according to the Brust-Schiffrin method in the absence of thiol molecules.<sup>2,28</sup> In this procedure, HAuCl<sub>4</sub> (3 mL, 30 mM) was first transferred from an aqueous solution to the organic phase (toluene) by (TOA)Br (8 mL, 50 mM) and then reduced by NaBH<sub>4</sub> (2.5 mL, 0.4 M) in the absence of thiol molecules. The organic phase was separated from the aqueous phase using a separation funnel. Excess NaBH<sub>4</sub> was quenched by addition of sulfuric acid (10 mL, 0.1 M). The organic phase was further washed by NaHCO<sub>3</sub> (10 mL, 1 M) and Milli-Q water. For details, see refs 2 and 28.

**Preparation of Samples.** Au(111) for both electrochemistry and STM were prepared by the method of Clavilier and Hamelin<sup>35</sup> and their quality checked by electrochemistry.<sup>33</sup> Prior to use, Au(111) electrodes were annealed in a hydrogen flame and quenched in Milli-Q water saturated with hydrogen gas. For AFM measurements, commercially available gold on glass samples were used and heated to red hot under a hydrogen flame prior to use. Clean electrodes were immediately transferred into thiol solutions for sample preparation. Thiol SAMs were formed by first immersing Au(111) electrodes in 0.5–1 mM thiol-containing ethanol, THF, or chloroform solutions at room temperature for several hours. For AuNP immobilization, after rinsing by Milli-Q water, ethanol, and toluene, the dithiol-modified electrodes were transferred to a solution containing TOA(Br) stabilized AuNPs for several hours to prepare the AuNP adlayer. Alkanethiol modification of immobilized AuNPs was achieved by first rinsing the electrodes by toluene and ethanol followed by immersion into a 0.5–1 mM ethanol solution of 1-tetradecanethiol for 1 h. Protein adlayers were prepared by immersing either the alkanethiol-modified Au(111) electrodes or the AuNP-modified electrodes into a NH<sub>4</sub>Ac (5 mM, pH 4.6) buffer containing azurin (24 μM) for several hours.

**Instrumentation and Measurements.** Electrochemical measurements were carried out at room temperature ( $23 \pm 2$  °C) using an Autolab system (Eco Chemie, The Netherlands) controlled by the general purpose electrochemical system (GPES). A three-electrode system consisting of a coiled platinum wire as the counter electrode (CE), a reversible hydrogen electrode (RHE) as the reference electrode (RE), and a Au(111)

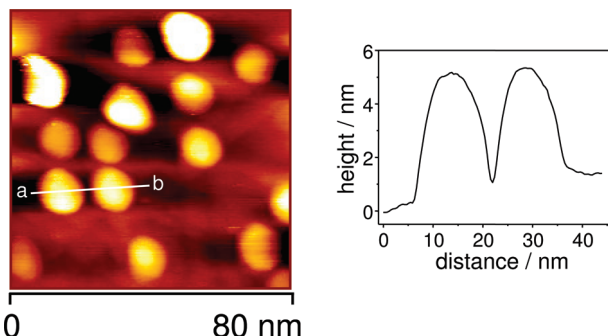


**Figure 1.** *Ex situ* STM image and corresponding cross section height profile of matrix isolated AuNPs on a BPDT/MPA-modified Au(111) surface. Image recorded in constant current mode under ambient conditions: Tunneling current  $I_t = 0.10$  nA and bias voltage  $V_b = -3.30$  V.

electrode as the working electrode (WE) was used. The working electrode was used in the hanging-meniscus mode.<sup>33</sup> The RHE was checked against a saturated calomel electrode (SCE) after each measurement. All potentials are reported versus the SCE. Purified argon (Chrompack, 5 N) was used to purge dioxygen from the solution before the measurements, and a gas stream was maintained over the solution during the measurements.

STM images were recorded in constant-current mode using a PicoSPM instrument (Molecular Imaging Co.) equipped with a bipotentiostat for potential control of both the substrate and tip. *In situ* imaging under potential control was conducted using a home-designed cell with a three-electrode system similar to that used for the electrochemical measurements.<sup>36</sup> STM tips were prepared from tungsten or Pt/Ir wires ( $\varnothing$  0.25 mm) by electrochemical etching, and insulated with Apiezon wax to eliminate Faradaic currents.<sup>36</sup> AFM images were recorded in air under ambient conditions using an Agilent 5500 atomic force microscope operated in contact mode. Cantilevers were Veeco model NP-S1, lever D, with  $k = 0.06$  N/m.

## 3. Results

**AuNP Assemblies on 4,4'-BPDT-Modified Au(111)-Electrode Surfaces.** The AuNPs synthesized as described, Scheme 1 and section 2, and immobilized on dithiol-modified gold electrodes were characterized by STM and AFM. Figure 1 shows a representative STM image (acquired in air under ambient conditions (*ex situ*) with corresponding cross section height profiles of individual AuNPs immobilized on a 1:1000 mixed monolayer of 4,4'-BPDT and 4-mercaptopbenzoic acid (MBA). The STM cross section profiles show a height of  $3.2 \pm 1$  nm which accords with previous findings on similarly prepared roughly spherical AuNPs based on TEM.<sup>18,27</sup> Some broadening in the apparent lateral size is seen. This could be caused by tip convolution or by drying artifacts caused by interactions between the AuNPs and the TOABr surface coating.

Figure 2 shows a contact mode AFM image of (TOA)Br stabilized AuNPs after immobilization on the 4,4'-BPDT-modified Au(111)-electrode surface in air. In comparison, Figure 3 shows an *in situ* STM image of the same system. Monolayers of uniform AuNP size are seen in both cases. The complementary information from AFM and STM is, however, also apparent. The lateral extension of the AuNPs is convoluted with the AFM tip in Figure 2. The apparent height is also smaller than the physical height, most likely due to the dense packing that does not enable the AFM tip to penetrate between the nanoparticles. The lateral AuNP dimension observed in the *in situ* STM images is about 5 nm, indicating that both the coating layer and the Au

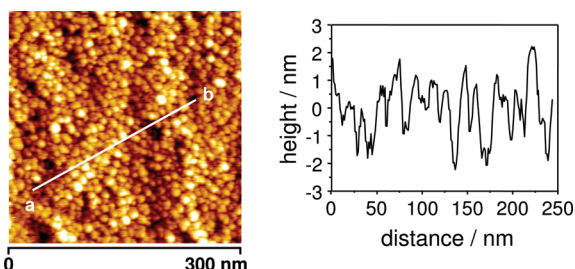


**Figure 2.** *Ex situ* AFM image and corresponding cross section height profiles of a densely packed AuNP monolayer on a BPDT-modified gold on glass surface. Image recorded in contact mode under ambient conditions.

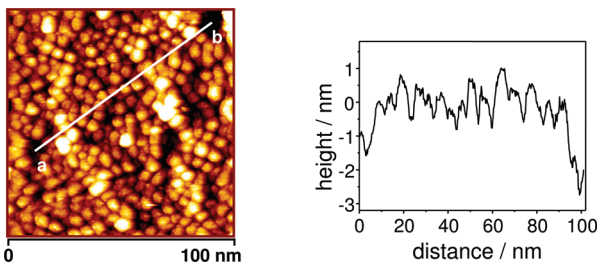


**Figure 3.** *In situ* STM image and corresponding cross section height profile of a densely packed AuNP monolayer on a BPDT-modified Au(111) surface. Image recorded in constant current mode. 20 mM ammonium acetate ( $\text{NH}_4\text{Ac}$ ) buffer at pH 4.6.  $I_t = 0.05 \text{ nA}$ ,  $V_b = -1.10 \text{ V}$ , and working electrode potential  $E_w = 0.33 \text{ V}$  vs SCE.

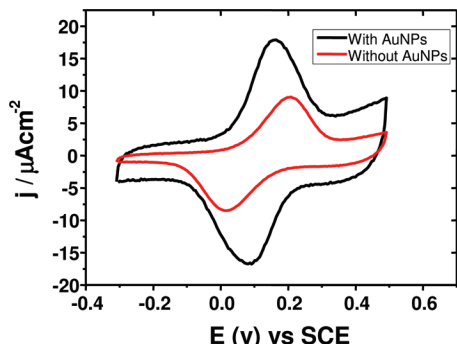


**Figure 4.** Cyclic voltammograms of an azurin submonolayer in configuration A (red line, with AuNPs) and B (black line, without AuNPs); cf. Scheme 2. Scan rate 3 V/s. 20 mM  $\text{NH}_4\text{Ac}$  buffer, pH 4.6.

core are recorded. The lateral dimension is also smaller and closer to the expected value than in AFM, cf. the AuNP height, perhaps indicative that the TOABr-coated AuNPs preserve their integrity better in the solute state. Overall, Figures 2 and 3 illustrate the local microenvironment in which the bound protein hybrids operate, with converging height dimensions from AFM and STM.

**Cyclic Voltammetry of Au(111)/4,4'-BPDT/AuNP/Azurin Molecular Assemblies.** Scheme 2 shows a view of the AuNP/azurin hybrid on the 4,4'-BPDT-modified Au(111)-electrode surface and of a reference system with azurin immobilized directly on a 1-tetradecanethiol-modified Au(111)-electrode surface. Figure 4 shows cyclic voltammograms of the Au/AuNP/azurin and of the Au/azurin reference system at a relatively low scan rate of 3 V s<sup>-1</sup>. The midpoint equilibrium potentials ( $E^0 = 120 \pm 5 \text{ mV}$  vs SCE) accord with reported values for azurin on variable-length alkanethiol monolayers.<sup>31–33</sup>

CVs of the AuNP/azurin hybrid system at larger scan rates, however, disclose composite voltammetric behavior, Figure 5.

The voltammetric peaks split into two pairs at scan rates larger than  $\approx 3 \text{ V s}^{-1}$ . Both sets of peaks follow the “trumpet form” of peak separation, Figure 6, strongly indicative of monolayer voltammetric behavior. The AuNP-free azurin reference system also gives trumpet plots but with a single pair of peaks only. The interfacial electrochemical ET rate constant,  $k_{app}$  (s<sup>-1</sup>), for the two “hybrid” processes and for azurin alone were determined from Laviron plots (Figure 6, bottom) of the peak separation  $\Delta E_p = (4RT/nF) \ln(1/2m)$ , where  $R$  is the gas constant,  $T$  the temperature,  $F$  Faraday’s constant, and  $n$  (=1) the number of electrons transferred. The parameter  $m$  is determined by  $k_{app}$  and the scan rate,  $v$  (V s<sup>-1</sup>), as  $m = RTk_{app}/nFv$ . The resulting values of  $k_{app}$  are collected in Table 1.

The voltammetric patterns and the values of the rate constants prompt several observations:

The voltammetric peak doublets are likely to represent two interfacial electrochemical processes. The close separation of the peaks and midpoint potentials similar to that of free azurin almost certainly mean that both processes are caused by interfacial ET between azurin and the electrode surface.

Within a factor of 2 or so, the rate constant associated with one of the voltammetric pairs (the “outer” pair) accords with the rate constant for azurin on the tetradecanethiol-modified Au(111)-electrode surface. The other rate constant, associated with the “inner” pair, is larger than that for the AuNP-free azurin reference system by a factor of more than 20.

The enhanced rate constant compares with that previously observed for AuNP/cyt c. The AuNP/protein binding modes are comparable in the two cases in the sense that both systems involve two strongly chemisorbed Au(111)–AuNP links and a strong noncovalent AuNP/protein link. The latter is electrostatic binding for AuNP/cyt c and hydrophobic binding for AuNP/azurin. We therefore assign the “inner” voltammetric pair and the enhanced ET rate constant to the “hybrid” unit with ET between azurin and the electrode via the AuNP.

The close similarity between the rate constant of the “outer” pair process and for direct ET of azurin via the 1-tetradecanethiol monolayer suggests that the “outer” pair is also caused by direct ET of azurin, but bypassing the AuNP. This would involve 4,4'-BPDT displacement on the Au(111)-electrode surface by 1-tetradecanethiol from the AuNP coating layer, giving similar covalent ET distances as for “direct” ET of azurin. Other mechanisms such as sterically hindered direct ET of azurin on the 4,4'-BPDT surface *between* the densely packed AuNPs are, however, also possible.

**In Situ STM of Au(111)/4,4'-BPDT/AuNP/Azurin Molecular Assemblies.** Figure 7 shows an *in situ* STM image of AuNP/azurin entities on the 4,4'-BPDT-covered Au(111)-electrode surface. Monolayers of separated uniform structures of the size of the AuNPs and azurin molecules are seen and height profiles shown. The potential control is supported by voltammograms of the AuNP/azurin hybrid surface directly in the electrochemical *in situ* STM cell, Figure 8.

Notably, **two** different *in situ* STM contrasts, i.e., a stronger and a weaker contrast, were consistently observed at submonolayer AuNP/azurin coverage, Figure 7. The stronger contrasts were robust in both size and time. The weaker contrasts showed a robust size distribution but some intensity variation in time, with indications of intensity fluctuations in successive scans. The presence of two different contrasts of comparable abundance accords with the two voltammetric signals of comparable intensity. Two contrast interpretations can be suggested. The weaker and fluctuating contrast is assigned to the AuNP/azurin hybrid in either case. In one interpretation, the robust stronger

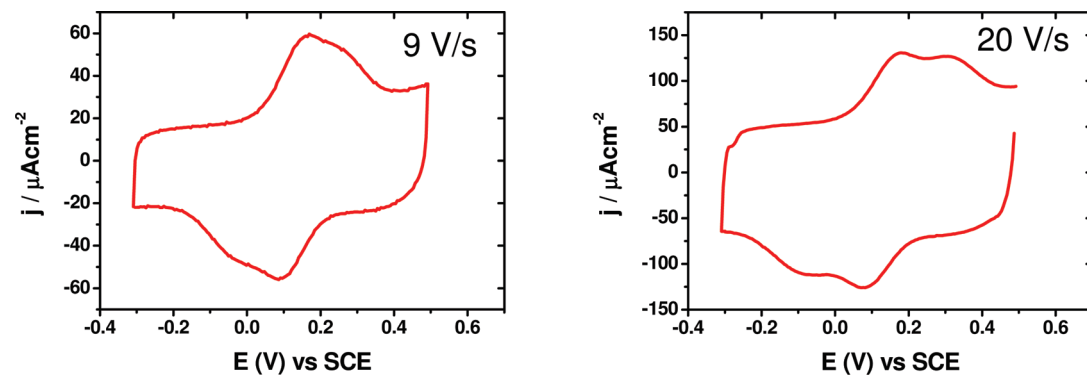


**Figure 5.** Cyclic voltammograms of azurin–AuNP hybrid structures at (A) 9 V/s and (B) 20 V/s. 20 mM NH<sub>4</sub>Ac buffer, pH 4.6.

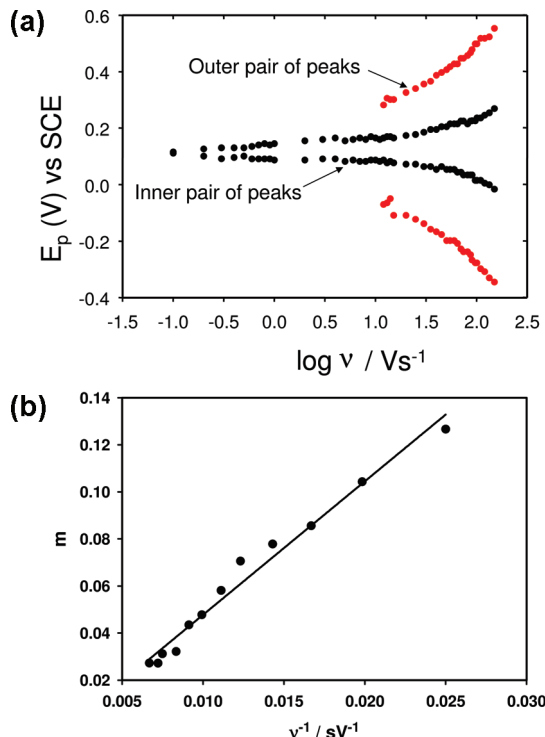
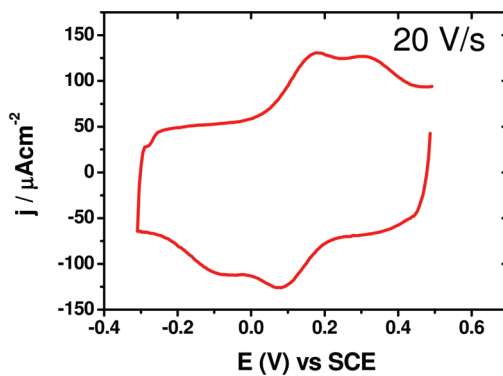


**Figure 6.** (top) Laviron trumpet plot of anodic and cathodic peak positions of azurin–AuNP hybrid structures immobilized on BPDT-modified Au(111) electrodes at varying scan rates. 20 mM NH<sub>4</sub>Ac buffer, pH 4.6. (bottom) Linear fit of the inner pair of peaks in the Laviron analysis. The parameter  $m = RTk_{app}/nFv$ ; cf. the text.

**TABLE 1: Formal Redox Potentials and Standard Interfacial Electrochemical Rate Constants for the Three Voltammetric Pairs of Azurin Signals**

| system   | $E^{\circ'} \text{ (mV)}$ | $k_{app} \text{ (s}^{-1}\text{)}$ |
|--|---------------------------|-----------------------------------|
| 1-tetradecanethiol–AuNP/Au(111)<br>(inner pair of peaks) | $120 \pm 5$               | $220 \pm 16$                      |
| 1-tetradecanethiol–AuNP/Au(111)<br>(outer pair of peaks) | $108 \pm 5$               | $4.9 \pm 0.4$                     |
| 1-tetradecanethiol/Au(111)                               | $110 \pm 5$               | $10.2 \pm 0.4$                    |

contrast is assigned to the AuNPs themselves, unbound from azurin. Alternatively, the stronger contrast could arise from azurin directly bound either to the 4,4'-BPDT adlayer or to 1-tetradecanethiol displaced from the AuNP coating to the Au(111)-electrode surface. The latter alternative accords best with the dual-peak voltammetry observed. Tunneling current/overpotential spectroscopy would be a route toward further distinction between these alternatives.



#### 4. Discussion

Arrays of coated molecular scale AuNPs have been brought to assemble in two-dimensional monolayers or submonolayers on Au(111)-electrode surfaces and characterized by CV and by AFM and *in situ* STM. As for the heme protein cyt *c*, the AuNP assembly has been brought further to operate as a platform for noncovalent binding of the blue copper protein azurin with an emerging 20-fold electrocatalytic rate constant increase compared with the AuNP-free tetradecanethiol azurin system. This is comparable to the electrocatalytic interfacial ET enhancement of cyt *c*.

The electrocatalytic binding modes of the two proteins resemble each other but differ in detail. The AuNP in the cyt *c* case was covalently linked to the Au(111)-electrode surface via amide bonding between a cysteamine monolayer on the Au(111)-electrode surface and the thioctic acid coating on the AuNP. Au–S bonding was the terminal contact both at the Au(111) surface and at the AuNP. AuNP binding in the azurin case is by chemisorption of the thiol groups of the 4,4'-biphenyldithiol monolayer to both the Au(111)-electrode surface and the AuNP. Protein binding to the AuNP is noncovalent in both cases. The binding is electrostatic for cyt *c* and hydrophobic for azurin. In spite of their noncovalent nature, protein attachment is strong in both cases and good electronic contact to the AuNP is ensured by the molecular orientation with the metal center facing the AuNP surface.

The CV patterns are, however, different. Cyt *c* gives a single electrocatalytically enhanced pair of peaks, although peak splitting at higher scan rates than could be recorded cannot be excluded. The strongly positively charged protein is also strongly repelled from the positively charged cysteamine layer between the immobilized AuNPs, with no direct ET between cyt *c* and the cysteamine covered Au(111)-electrode surface. Both the protein surface around the Cu site and the local AuNP and Au(111)-electrode surface environment are quite different for azurin and dominated by hydrophobic interactions. As a result, azurin can interact closely both with the hydrophobically coated AuNP and with the 4,4'-BPDT supporting layer. The latter interaction could be purely hydrophobic azurin contact with the aromatic ring system, or involve displacement of surface-bound 4,4'-BPDT with 1-tetradecanethiol followed by azurin binding to the latter. Scrambling of the thiol groups of the 4,4'-BPDT layer with the azurin disulfide group is less likely. As a consequence, two pairs of voltammetric peaks emerge at high scan rates. The interfacial ET rate associated with one set of peaks corresponds closely to the reference system of azurin bound directly to a 1-tetradecanethiol monolayer, the other set to a 20 times enhanced rate constant which we assigned to AuNP-bound azurin. *In situ* STM offers support for a dual

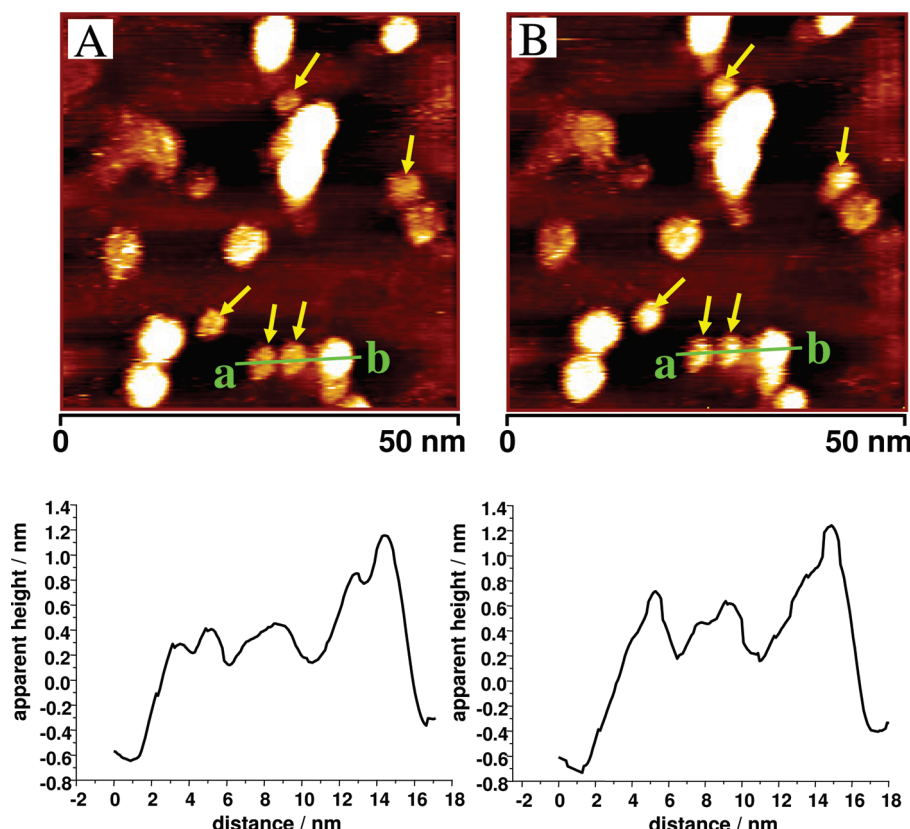


**Figure 7.** *In situ* STM images, top, and cross section profiles along the line ab, bottom, of the AuNP/azurin submonolayer. Part B was recorded 40 s after part A. The images systematically show assemblies of strong and weak contrasts, the latter fluctuating in time. The intensities marked by yellow arrows almost double from image A to image B, while other weak contrast intensities are reduced. 20 mM NH<sub>4</sub>Ac, pH 4.6.  $I_t = 0.03$  nA,  $V_b = -0.523$  V, and  $E_w = 0.29$  V vs SCE.

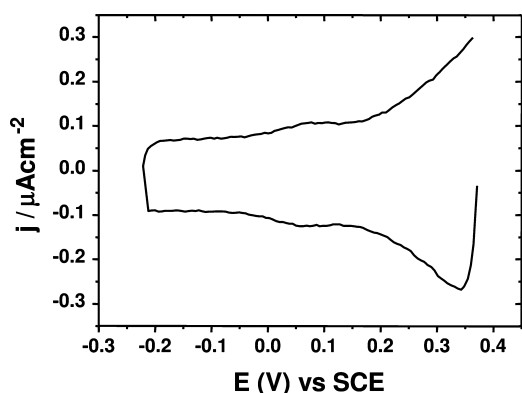
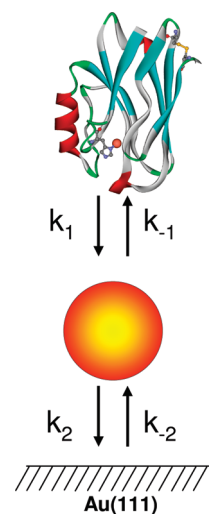


**Figure 8.** Cyclic voltammogram of matrix isolated azurin–AuNP hybrid structures immobilized on a Au(111) surface. Recorded in the *in situ* STM cell. 20 mM NH<sub>4</sub>Ac, pH 4.6. Scan rate 1 V/s. The peak around 0.08 V is due to azurin oxidation and reduction with an increasing capacitive background toward positive potentials. The scan is reversed at 0.4 V.

interfacial ET pattern of azurin on the AuNP assembly. The robust stronger contrast was assigned to azurin directly bound to the (4,4'-BPDT or 1-tetradecanethiol) modified Au(111)-electrode surface, while the weaker, fluctuating contrast was assigned to the hybrid of azurin and the 1-tetradecanethiol-coated AuNP.

The two-step interfacial ET mechanism proposed in our previous communication would also apply to the AuNP/azurin system, Scheme 3. This scheme at first resembles electrochemical ET patterns of proteins with two metal centers with intramolecular ET between the centers. Cytochrome *c*<sub>4</sub><sup>37</sup> and Cu-nitrite oxidase<sup>38,39</sup> are such examples. There is, however, a

### SCHEME 3: Schematic Representation of the Two-Step ET Process in the Au/AuNP/Szurin System



notable difference from “natural” two-center proteins, for which intramolecular interfacial ET rate constants are in the ms to tens of ms time ranges. Voltammetric peak shape and the prevalence of a single peak of the two-step AuNP/protein process point to much faster interfacial ET for either the AuNP/electrode or the AuNP/protein transition. Together with observed electrocatalysis of simple electrochemical ET processes by molecular scale AuNPs,<sup>9,10,17,18,20–23</sup> this leaves issues as to the physical mechanism of the AuNP catalyzed interfacial ET.

Viewing the AuNP catalyzed ET process as a “normal” two-step ET process leaves the reorganization free energy and

electronic couplings of the AuNP to the Au(111)-electrode surface and to the protein in focus. Reasons *why* the reorganization free energy should be significantly lower or the electronic coupling factors larger compared with direct interactions of azurin with the electrode surfaces over shorter distances are, however, not obvious. It could be argued that electronically favorable conformational changes in the linker groups are induced by the presence of the AuNP, but there is no support for such a conjecture.

The observed small but systematic broadening of the AuNP plasmon band on cyt *c* binding noted in our previous report<sup>18</sup> offers a clue. The broadening accorded with ultrafast ( $\approx 10^{13}$  s<sup>-1</sup>) ET from excited AuNP plasmon states to (oxidized) bound cyt *c*. Interfacial AuNP/molecule ET, although here involving excited electronic states, can thus be fast even over the  $\approx 1$  nm thioctic acid binding length. Such charge transfer “resonances” carry over to the AuNP interfacial ET rate enhancement, illustrated by the following superexchange view of the electrochemical (here cathodic) current<sup>40,41</sup>

$$i_{\text{cath}} \propto \frac{\int \int d\epsilon_{\text{elect}} d\epsilon_{\text{part}} f(\epsilon_{\text{elect}})[1 - f(\epsilon_{\text{part}})] f(\epsilon_{\text{part}}) \times \Delta_{\text{elect,part}} \Delta_{\text{part,mol}}}{(\epsilon_{\text{elect}} - \epsilon_{\text{part}})^2 + (\Delta_{\text{elect,part}} + \Delta_{\text{part,mol}})^2} \times \exp\left[-\frac{\Delta G^{\ddagger}(E_r; \eta; \epsilon_{\text{elect}}, \epsilon_{\text{part}})}{k_B T}\right] \quad (1)$$

$\epsilon_{\text{elect}}$  and  $\epsilon_{\text{part}}$  and  $f(\epsilon_{\text{elect}})$  and  $f(\epsilon_{\text{part}})$  are the electronic energies and the Fermi functions of the electrode and the AuNP, respectively, while  $\Delta_{\text{elect,part}}$  and  $\Delta_{\text{part,mol}}$  are the electronic couplings between the electrode and the AuNP and the AuNP and the molecule, respectively.  $\Delta G^{\ddagger}(E_r; \eta; \epsilon_{\text{elect}}, \epsilon_{\text{part}})$  is the activation Gibbs free energy that depends on the reorganization free energy,  $E_r$ , for ET to the azurin molecule and the overpotential  $\eta$ .  $k_B$  is Boltzmann’s constant and  $T$  the temperature. Rate constant forms involving a continuous distribution of intermediate state electronic energy levels were in fact introduced early.<sup>41</sup> Equation 1 is equivalent to representations of the “chemical mechanism” of SERS.<sup>24,25</sup> In both cases, the energy denominator opens resonance channels here ET channels in energy ranges where  $\epsilon_{\text{elect}}$  and  $\epsilon_{\text{part}}$  coincide. The appropriate dominating ranges of the continuous energy distributions of the electrode and the AuNP are close to the Fermi levels of the electrode and the AuNP and both thermally accessible. In addition, electronic coupling effects ( $\Delta_{\text{elect,part}}$  and  $\Delta_{\text{part,mol}}$ ) would be enhanced by surface plasmonic delocalization<sup>24,25</sup> compared to direct interfacial ET between the surface-modified Au(111)-electrode surface and azurin. This is quite different from molecular (nonredox) linkers for which the HOMO and LUMO energies are strongly off-resonance with energy levels around the Fermi levels of the electrode and the AuNP. A more precise analysis of eq 1 will be given elsewhere.

As a final observation, AuNPs in the plasmonic size range,  $\geq 2.5$  nm, are expectably needed for high interfacial electrocatalytic efficiency of AuNPs in the superexchange mode over a broad potential range. Smaller AuNPs would be charged by single-ET with dips in the charging currents and in electrocatalytic overpotential profiles. A likely consequence of single-electron charging is that AuNP charging resembles molecular oxidation and reduction with corresponding substantial solvent reorganization. This would further lower the interfacial ET rate constants of the AuNP in the electrocatalytic sequence.

**Acknowledgment.** Financial support from the National Danish Research Council for Technology and Production Sciences, the Lundbeck Foundation, the Carlsberg Foundation, and Brødrene Hartmann’s Foundation is acknowledged.

## References and Notes

- Schmid, G. *Chem. Rev.* **1992**, *92*, 1709–1727.
- Brust, M.; Walker, M.; Bethell, D.; Schiffrin, D. J.; Wyman, R. *J. Chem. Soc., Chem. Commun.* **1994**, 801–802.
- Brust, M.; Fink, J.; Bethell, D.; Schiffrin, D. J.; Kiely, C. *J. Chem. Soc., Chem. Commun.* **1995**, 1655–1656.
- Templeton, A. C.; Wuelfing, W. P.; Murray, R. W. *Acc. Chem. Res.* **2000**, *33*, 27–36.
- Rao, C. N. R.; Kulkarni, G. U.; Govindaraj, A.; Satishkumar, B. C.; Thomas, P. *J. Pure Appl. Chem.* **2000**, *72*, 21–33.
- Daniel, M.-C.; Astruc, D. *Chem. Rev.* **2004**, *104*, 293–346.
- Burda, C.; Chen, X.; Narayanan, R.; El-Sayed, M. A. *Chem. Rev.* **2005**, *105*, 1025–1102.
- Zhao, J.; Bradbury, C. R.; Huclova, S.; Potapova, I.; Carrara, M.; Fermin, D. J. *J. Phys. Chem. B* **2005**, *109*, 22985–22994.
- Bradbury, C. R.; Zhao, J.; Fermin, D. J. *J. Phys. Chem. C* **2008**, *112*, 10153–10160.
- Zabet-Khosousi, A.; Dhirani, A.-A. *Chem. Rev.* **2008**, *108*, 4072–4124.
- Rotello, V., Ed. *Nanoparticles: Building Blocks for Nanotechnology*; Springer: New York, 2004.
- Quinn, B. M.; Liljeroth, P.; Ruiz, V.; Laaksonen, T.; Kontturi, K. *J. Am. Chem. Soc.* **2003**, *125*, 6644–6645.
- Laaksonen, T.; Ruiz, V.; Liljeroth, P.; Quinn, B. M. *Chem. Soc. Rev.* **2008**, *37*, 1836–1846.
- Delfino, I.; Cannistraro, S. *Biophys. Chem.* **2009**, *139*, 1–7.
- Chen, S.; Pei, R. *J. Am. Chem. Soc.* **2001**, *123*, 10607–10615.
- Chen, S. *J. Mater. Chem.* **2007**, *17*, 4115–4121.
- Murray, R. W. *Chem. Rev.* **2008**, *108*, 2688–2720.
- Jensen, P. S.; Chi, Q.; Grumsen, F. B.; Abad, J. M.; Horsewell, A.; Schiffrin, D. J.; Ulstrup, J. *J. Phys. Chem. C* **2007**, *111*, 6124–6132.
- Bond, G. C.; Louis, C.; Thompson, D. T. *Catalysis by Gold*; Imperial College Press: London, 2006.
- (a) Jiang, X.; Jiang, J.; Jin, Y.; Wang, E.; Dong, S. *Biomacromolecules* **2005**, *6*, 46–53. (b) Jiang, X.; Shang, L.; Wang, Y.; Dong, S. *Biomacromolecules* **2005**, *6*, 3030–3036.
- (a) Liu, T.; Zhong, J.; Gan, X.; Fan, C.; Li, G.; Matsuda, N. *ChemPhysChem* **2003**, *4*, 1364–1366. (b) Pradeep, T.; Tom, R. T. *Langmuir* **2005**, *21*, 11896–11902.
- Xiao, Y.; Patolsky, F.; Katz, E.; Hainfeld, J. F.; Willner, I. *Science* **2003**, *299*, 1877–1881.
- Katz, E.; Willner, I. *Angew. Chem., Int. Ed.* **2004**, *43*, 6042–6108.
- Malshukov, A. G. In *The Chemical Physics of Solvation. Part C. Solvation in Specific Physical, Chemical and Biological Systems*; Dogonadze, R. R., Kálmán, E., Kornyshev, A. A., Ulstrup, J., Eds.; Elsevier: Amsterdam, The Netherlands, 1988; pp 433–479.
- (a) Kneipp, K.; Wang, Y.; Kneipp, H.; Perelman, L. T.; Itzkan, I.; Dasari, R. R.; Feld, M. S. *Phys. Rev. Lett.* **1997**, *78*, 1667–1670. (b) Kneipp, K.; Kneipp, H.; Itzkan, I.; Dasari, R. R.; Feld, M. S. *Chem. Rev.* **1999**, *99*, 2957–2975.
- Zhang, J.; Kuznetsov, A. M.; Medvedev, I. G.; Chi, Q.; Albrecht, T.; Jensen, P. S.; Ulstrup, J. *Chem. Rev.* **2008**, *108*, 2737–2791.
- Albrecht, T.; Guckian, A.; Kuznetsov, A. M.; Vos, J. G.; Ulstrup, J. *J. Am. Chem. Soc.* **2006**, *128*, 17132–17138.
- Abad, J. M.; Mertens, S. F. L.; Pita, M.; Fernández, V. M.; Schiffrin, D. J. *J. Am. Chem. Soc.* **2005**, *127*, 5689–5694.
- Aubin-Tam, M.-E.; Hamad-Schifferli, K. *Langmuir* **2005**, *21*, 12080–12084.
- Haiss, W.; Wang, C.; Jitchati, R.; Grace, I.; Martin, S.; Batsanov, A. S.; Higgins, S. J.; Bryce, M. R.; Lambert, C. J.; Jensen, P. S.; Nichols, R. J. *J. Phys. C: Condens. Matter* **2008**, *20*, 374119.
- Chi, Q.; Zhang, J.; Andersen, J. E. T.; Ulstrup, J. *J. Phys. Chem. B* **2001**, *105*, 4669–4679.
- (a) Chi, Q.; Farver, O.; Ulstrup, J. *Proc. Natl. Acad. Sci. U.S.A.* **2005**, *102*, 16203–16208. (b) Chi, Q.; Zhang, J.; Jensen, P. S.; Christensen, H. E. M.; Ulstrup, J. *Faraday Discuss.* **2006**, *131*, 181–195.
- Chi, Q.; Zhang, J.; Friis, E. P.; Andersen, J. E. T.; Ulstrup, J. *Electrochim. Commun.* **1999**, *1*, 91–96.
- Friis, E. P.; Andersen, J. E. T.; Madsen, L. L.; Møller, P.; Bonander, N.; Ulstrup, J. *Electrochim. Acta* **1997**, *42*, 2889–2897; **1998**, *43*, 1113–1122 (erratum).
- (a) Clavilier, J.; Faure, R.; Guinet, G.; Durand, R. *J. Electroanal. Chem.* **1980**, *107*, 205–209. (b) Hamelin, A. *J. Electroanal. Chem.* **1996**, *411*, 1–12.

- (36) Zhang, J.; Chi, Q.; Nielsen, J. U.; Friis, E. P.; Andersen, J. E. T.; Ulstrup, J. *Langmuir* **2000**, *16*, 7229–7237.
- (37) Karlsson, J.-J.; Nielsen, M. F.; Thuesen, M. H.; Ulstrup, J. *J. Phys. Chem. B* **1997**, *101*, 2430–2436.
- (38) Zhang, J.; Welinder, A. C.; Hansen, A. G.; Ulstrup, J. *J. Phys. Chem. B* **2003**, *107*, 12480–12484.
- (39) Welinder, A. C.; Zhang, J.; Hansen, A. G.; Moth-Poulsen, K.; Christensen, H. E. M.; Bjørnholm, T.; Ulstrup, J. *Z. Phys. Chem.* **2007**, *221*, 1343–1378.
- (40) Haiss, W.; Albrecht, T.; van Zalinge, H.; Higgins, S. J.; Bethell, D.; Höbenreich, H.; Schiffrin, D. J.; Nichols, R. J.; Kuznetsov, A. M.; Zhang, J.; Chi, Q.; Ulstrup, J. *J. Phys. Chem. B* **2007**, *111*, 6703–6712.
- (41) (a) Dogonadze, R. R.; Ulstrup, J.; Kharkats, Yu. I. *J. Electroanal. Chem.* **1973**, *43*, 161–174. (b) Dogonadze, R. R.; Ulstrup, J.; Kharkats, Yu. I. *J. Theor. Biol.* **1973**, *40*, 259–277.

JP902611X